PERGAMON

Atmospheric Environment 34 (2000) 2975–2982

ATMOSPHERIC ENVIRONMENT

www.elsevier.com/locate/atmosenv

Effects of subgrid segregation on ozone production efficiency in a chemical model

Jinyou Liang, Mark Z. Jacobson*

Department of Civil and Environmental Engineering, Stanford University, Stanford, CA 94305-4020, USA

Received 20 April 1999; accepted 8 November 1999

Abstract

Ozone production efficiency is a parameter used for evaluating the effect of anthropogenic NO_x on tropospheric ozone. For this work, zero-dimensional simulations were run to compare the differences in ozone production efficiency when air masses of different origin were separated and when they were merged. The purpose of the simulations was to estimate whether coarsely resolved models might under or overpredict ozone production due to their blending of air masses of different origin. Cases were run for several combinations of air mass origin, different latitudes, times of year, air mass dilution ratios and initial gas concentrations. The main result of this study is that integrated ozone production may be overpredicted by as much as 60% in coarse-model grid cells exposed to different air masses. Under certain conditions, such as in rather finely resolved urban airshed models, ozone production may actually be underpredicted by about 20% in mid-latitudes during summer. The results imply that large-scale global models may have a difficult time correctly predicting ozone concentrations near, for instance, urban/free tropospheric boundaries, a conclusion supported by other studies examining parameters other than ozone production efficiency.

Keywords: Ozone; Air pollution modeling; Photochemistry; Atmospheric modeling

1. Introduction

Atmospheric models that simulate chemistry are subject to errors that arise from uncertainties in estimating concentrations of trace species. The errors originate partly from the use of a condensed reaction mechanism, partly from the use of approximate photochemical reaction rate coefficients, and partly from missing processes or reactions. Unaccounted-for inhomogeneity in emission rates and land cover type within a model grid cell may also contribute to errors.

Aside from the missing processes or reactions, the other three sources of errors have different characteristics. The first source depends on the method of reducing the chemical mechanism (e.g., Makar and Polavarapu, 1997), but it may be controlled by applying a quantitative criterion to the truncation of the comprehensive reaction mechanism. Liang and Jacobson (1999) presented an example of applying a criterion to develop a compressed chemical mechanism for the oxidation of SO_2 from a larger gas-aqueous photochemical mechanism. The criterion was that 95% of the total production and loss rates of important species calculated using the larger reaction mechanism were accounted for by the compressed chemical mechanism at any instant during the calculation. The resulting deviations in concentrations of targeted species between the compressed and expanded mechanisms were less than 10%. The second source of errors, photochemical rate coefficient data, is independent of the model, and will decrease as more laboratory data become available. The third source of error results from inadequate description of mixing processes occurring within a grid cell of a chemical-transport model.

Hilst (1998) illustrated the importance of the effects of inhomogeneous mixing on chemical reaction rates at a time scale of 10–1000 s by using exact solutions and

* Corresponding author. Tel.: +1-650-723-6836; fax: +1-650-725-9720.

E-mail address: jacobson@ce.stanford.edu (M.Z. Jacobson).

1352-2310/00/$ - see front matter
PII: S1352-2310(99)00520-8

a second-order closure scheme for several chemical kinetic equations, to find that the volume-averaged reaction rates in segregated systems can vary by orders of magnitude compared with the rates predicted for a uniformly mixed reactor system.

Chatfield and Delany (1990) in a unique study used a one-dimensional time-dependent model to simulate the effect of plume convection on ozone production in the tropics, and found that the dilution, principally due to vertical transport, may significantly increase the efficiency of ozone production. In a pioneering study, Sillman et al. (1990) developed a subgrid module to account for the heterogeneity of trace gases within a grid cell of a three-dimensional model. This scheme has been used in the prediction of rural ozone distributions in the US (Jacob et al., 1993; Liang et al., 1998; Horowitz et al., 1998) Jang et al. (1995) used a three-dimensional model with adaptive grid resolution to find that increasing the grid resolution may increase or decrease modeled time series of maximum ozone concentrations at specific sites. The latter study discussed a different issue from that discussed here, as shown below. Poppe et al. (1998) recently studied the influence of atmospheric dilution on ozone formation in biomass burning plumes, to find that the effects of dilution on the maximum ozone mixing ratio and on the amount of ozone formed in the entire plume depend strongly on the time scale and the final value of the dilution. They suggested a substantial uncertainty of model predicted ozone formation from biomass burning plumes. Their study differs from this study in that we look at abrupt mixing, associated particularly with lack of resolution in global models, of air masses of different geographic origin, and in that we look at the effect on ozone production efficiency.

Ozone production efficiency may be defined as the number of ozone molecules produced per $NO_x = NO + NO_2$ molecule lost to form nitric acid, peroxyacylnitrates, and organic nitrates (e.g. Lin et al., 1988), or as the number of ozone molecules produced per nitric acid molecule formed (Liu et al., 1987). Both definitions reveal the coupling between a basin-wide, regional, or global production of volume-integrated ozone and the corresponding total emissions of NO_x. Related, but different, parameters are the spatial and temporal distribution of ozone maxima, normalized gross errors/biases of ozone predictions, and the probability of peak ozone concentrations. All parameters of ozone concentration and ozone production efficiency are important for simulations aimed at evaluating the attainment of ozone air quality standards at specific sites. Studies of ozone production and, therefore, ozone concentration should also address the loss of NO_x since ozone production is limited by the availability of NO_x in much of the troposphere (Chameides et al., 1992). For example, if ozone production and concentration are well simulated at a site for a period but the loss of NO_x is underpredicted (overpredicted) during the same period, the model will then overpredict (underpredict) the ozone production efficiency and more (less) NO_x will be retained in the model to produce more (less) ozone elsewhere or later at the site. Hence, the use of ozone production efficiency is especially useful for coupling ozone production with the loss of NO_x and with emissions of NO_x in locations where air masses of different origin are adjacent to each other. We use a zero-dimensional photochemical model to illustrate the sensitivity of ozone production efficiency, as defined by Lin et al. (1988), to the assumption of uniform mixing in a tropospheric chemical model. The use of the other definition was also applied, but we found that it did not alter our conclusions. We describe the method of our investigation in Section 2, and present our findings in Section 3.

2. Model and simulations

We use a zero-dimensional photochemical model (Liang and Jacob, 1997; Liang and Jacobson, 1999) to investigate the CH_4–C_2H_6–C_3H_8–C_4H_{10}–C_3H_6–Isoprene-CO–NO_x photochemical system (Horowitz et al., 1998). The species defining the chemical environment are listed in Table 1 and are solved using an implicit iterative method described in Liang and Jacobson (1999). Aqueous-phase chemistry is neglected since it should not alter our conclusions below. The effects of aqueous-phase cloud chemistry on ozone production efficiency in the troposphere has been found to be small (Liang and Jacob, 1997), and the effect of aqueous-phase aerosol chemistry on ozone is negligible due to its small liquid water content.

We run six cases to represent a range of atmospheric conditions. The six cases are (1) baseline urban/baseline land, (2) fresh urban/baseline land, (3) aged urban/baseline land, (4) baseline land/ocean, (5) polluted land/ocean, and (6) forest land/ocean, and the initial composition of various air parcels are listed in Table 2. Each of the six cases consists of 12 runs that represent January, April, July, and October at the equator, 30, and 60°N. Each run was conducted for dilution ratios (the air mass in the dilute air parcel to that in the concentrated air parcel) of 1, 2, 4, 8, 16, 32, 64, and 128. These ratios were chosen since concentrated to dilute air mass ratios have been shown to range from < 1 to 50% in a three-dimensional chemical transport model over North America (Liang et al., 1998). For each run, we simulated temporal transformations of two air parcels when they were isolated from each other and when they were mixed with different dilution ratios. We suggest that this procedure is a helpful approach for studying the effects of lack of resolution in a large-scale model on ozone production efficiency. Suppose a coarsely resolved model grid cell covers a polluted urban region and nonpolluted land region. The

Table 1
Species defining the chemical environment

Oxidants			
1.	O_3(g)	2.	O(g)
3.	$O(^1D)$(g)	4.	OH(g)
5.	HO_2(g)	6.	H(g)
7.	H_2O_2(g)		
Nitrogen compounds			
8.	NO_2(g)	9.	NO(g)
10.	HNO_2(g)	11.	HNO_4(g)
12.	NO_3(g)	13.	N_2O_5(g)
Primary organic species			
14.	CH_4(g)	15.	C_2H_6(g)
16.	C_3H_8(g)	17.	C_4H_{10}(g)
18.	C_3H_6(g)	19.	C_5H_8(g)
Secondary organic species			
20.	CO(g)	21.	HCOOH(g)
22.	HCHO(g)	23.	O_2CH_2OH(g)
24.	CH_3O_2(g)	25.	CH_3OOH(g)
26.	CH_3OH(g)	27.	$C_2H_5O_2$(g)
28.	CH_3CO_3(g)	29.	$CH_3C(O)O_2NO_2$(g)
30.	CH_3CHO(g)	31.	C_2H_5OH(g)
32.	C_2H_5OOH(g)	33.	CH_3COOH(g)
34.	$CH_3C(O)OOH$(g)	35.	$CH_3CH_2CH_2OO$(g)
36.	CH_3COCH_3(g)	37.	$HOCH_2C(O)OO$(g)
38.	$CH_3COCH_2O_2$(g)	39.	$CH_3CH(OO)CH_3$(g)
40.	HCOHC(O)OO(g)	41.	HCOHC(O)OOH(g)
42.	$HCOHC(O)OONO_2$(g)	43.	$HOCH_2CHO$(g)
44.	$HOCH_2(CH_3)=CHCHO$(g)	45.	$HOCH_2CO_2(CH_3)CH(OH)CHO$(g)
46.	$HOCH_2COOH(CH_3)CH(OH)CHO$(g)	47.	$NO_3C_5H_8O_2$(g)
48.	$NO_3C_5H_8OOH$(g)	49.	$CH_2(OH)COO(CH_3)CH(ONO_2)CH_2OH$(g)
50.	$CH_2=C(CH_3)CH(ONO_2)CH_2OH$(g)	51.	$ISNO_3$(g)[a]
52.	$CH_2(OH)COOH(CH_3)CH(ONO_2)CH_2OH$(g)	53.	$NO_3CH_2CH(OO)CH_3$(g)
54.	$C_2H_4(OO)COCH_3$(g)	55.	$CH_2=C(CH_3)CHO$(g)
56.	$NO_3CH_2C(OO)(CH_3)CHO$(g)	57.	$CH_2=C(CH_3)C(O)OO$(g)
58.	$CH_2=C(CH_3)C(O)OOH$(g)	59.	$C_2H_5C(O)CH_3$(g)
60.	CH_3COCHO(g)	61.	CH_3NO_3(g)
62.	$HOCH_2C(OO)(CH_3)CHO$(g)	63.	$HOCH_2C(OOH)(CH_3)CHO$(g)
64.	$CH_3COCH=CH_2$(g)	65.	$CH_3COCH(OO)CH_2NO_3$(g)
66.	$CH_2=C(CH_3)C(O)OONO_2$(g)	67.	$HOC_3H_6O_2$(g)
68.	HOC_3H_6OOH(g)	69.	$CH_3CH_2C(O)OONO_2$(g)
70.	CHOCHO(g)	71.	$HOCH_2C(O)OOH$(g)
72.	$NO_3CH_2CH(OOH)CH_3$(g)	73.	$C_4H_8(OO)OONO$(g)
74.	C_4H_9OONO(g)	75.	C_4H_9OO(g)
76.	C_4H_9OOH(g)	77.	$CH_3CH_2CH_2OOH$(g)
78.	$CH_3CH(OOH)CH_3$(g)	79.	C_2H_5CHO(g)
80.	$CH_3CH_2C(O)OO$(g)	81.	C_2H_5COOH(g)
82.	HOC_5H_8OO(g)	83.	HOC_5H_8OOH(g)
84	C_3H_7OH(g)	85.	$CH_3CH_2C(O)OOH$(g)
86.	$CH_3COCH(OO)CH_2OH$(g)	87.	$CH_3COCH(OOH)CH_2OH$(g)
88.	$HOCH_2C(O)OONO_2$(g)	89.	$CH_2(OH)C(O)CH_3$(g)

[a]Stable organic nitrate.

model assumes all emissions are immediately diluted within the grid cell over the polluted and nonpolluted areas. In reality, the air masses may be relatively isolated although dilution occurs slowly over time. The simulations we compare include those in which the air masses are completely isolated, and the rest in which the air masses are completely merged, but at different ratios of the size of one air mass to the other. If the air masses truly

Table 2
Initial conditions of air parcels[a]

Species	Baseline urban	Fresh urban	Aged urban	Baseline land	Polluted land	Forest land	Ocean
O_3	60	60	120	30	60	30	30
NO_x	20	50	5	0.5	2	0.5	0.05
SO_2	2	2	0.2	0.2	0.2	0.2	0.01
CO	500	500	200	100	200	100	100
C_2H_6	5	5	2	2	2	2	1
C_3H_8	2.5	5	1	1	1	1	0.1
C_3H_6	2.5	5	1	0.1	0.1	0.1	0.01
C_4H_{10}	10	20	4	1	1	1	0.05
C_5H_8	0.1	0.1	0.1	0.5	0.5	2	0.01
H_2O_2	5	2	10	1	2	1	1
HCHO	2.5	1	10	1	2	1	0.1
CH_3CHO	1	0.5	5	0.5	1	0.5	0.1

[a]The unit of chemical compounds is ppbv. The starting time of integration was 6 am. Simulations were conducted for six cases: (1) baseline urban/baseline land, (2) fresh urban/baseline land, (3) aged urban/baseline land, (4) baseline land/ocean, (5) polluted land/ocean, and (6) forest land/ocean. In each of the above cases, the air-parcel pair were integrated separately, and the results were weighted according to airmass ratios by $1:2^{n-1}$($n = 1$–8) to obtain the results representing the isolated simulation. For the mixed simulation, initial conditions were obtained by weighting the air-parcel pair according to airmass ratios. The altitude is 1.5 km. For each simulation, 12 runs were conducted representing January, April July, and October at the equator, 30 and 60°N, respectively. Ozone columns (temperatures) are 240(289), 250(289), 255(288), 245(288) for January, April, July, and October at the equator, 280(281), 305(282), 285(288), 270(284) at 30°N and 370(256), 430(263), 340(276), 300(267) at 60°N. Ozone columns are in Dobson Unit (2.687×10^{16} molecules cm^{-2}), and temperatures are in Kelvin.

remain isolated, then the difference in ozone production efficiency between the isolated and merged cases are errors arising from not resolving a three-dimensional model. We choose a maximum isolation time for the isolated simulations of 10 h noting that, in reality, dilution of isolated air masses in a single grid cell of a coarse model will probably occur in less than this time period. For the simulations, we assume that each dilution ratio is constant in time but note that, in reality, dilution ratios change. To account for this effect, we present results for several dilution ratios.

3. Effects of subgrid heterogeneity on ozone production efficiency

Fig. 1 shows the growth curves of ozone and NO_x in the fresh urban/baseline land case at 30°N in July. The net ozone produced is minimal in the baseline land air parcel (line 1, top) and 120 ppbv in the fresh urban air parcel (line 2, top) during daytime. When the two air parcels are well mixed, the net ozone produced during daytime decreased from 60 to 20 ppbv when the mass ratio of the baseline land air parcel to the fresh urban air parcel increased from 1 to 8 (lines 3–6, top). NO_x concentration decreased from 50 ppbv to a few ppbv during daytime in the fresh urban air parcel (line 2, bottom).

Two important quantities for ozone production efficiency are the gross ozone production (mainly through the reactions of NO with peroxy radicals) and the net loss of NO_x (mainly through the formation of nitric acid and the net formation of peroxyacylnitrates and organic nitrates). Figs. 2 and 3 show the ratios of gross ozone production and the net loss of NO_x in the mixed simulation to those in the isolated simulation for the fresh urban/baseline land case at 30°N in July. The quantity shown is cumulative e.g., summed from 0 to 1 h for the value at 1 h of simulation at the x-axis. The ratios exceed unity in all cases, namely, both gross ozone production and the net loss of NO_x are enhanced in the mixed simulation compared with those in the isolated simulation, reflecting that the cycling of OH and HO_2 radicals are more efficient in the mixed simulation than in the isolated simulation.

Fig. 4 shows the percentage difference between ozone production efficiencies in the mixed simulations and those weighted sums in the isolated simulations for the fresh urban/baseline land case at 30°N and 50°N in January, July, and October. Note that the case for 30°N in July can also represent that for tropical clear-sky situation, due to the similar actinic fluxes in both cases. It is shown that the ratios are larger than unity in most situations, except in July and when the isolation time was shorter than a few hours. We discuss in the appendix that ozone production efficiency may be either overestimated or underestimated in the mixed simulation compared with that in the isolated simulation. Because of this, the percentage difference between gross ozone production

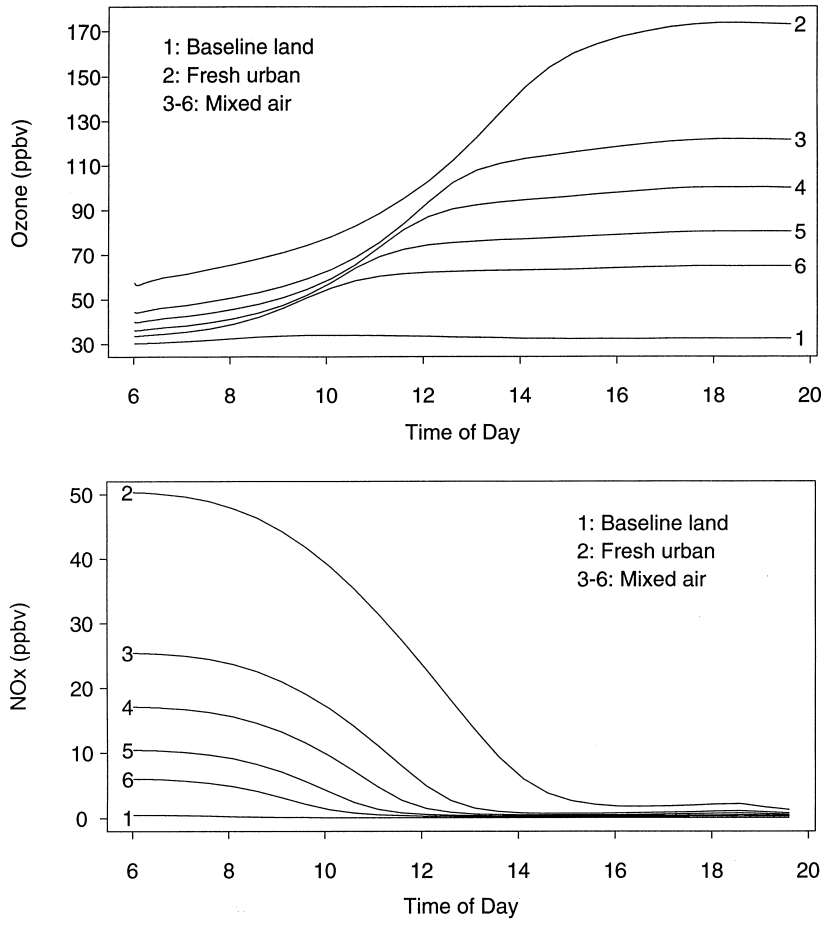

Fig. 1. Ozone (top) and NO_x (bottom) growth curves for the fresh urban/baseline land case at 30°N in July. A dilute (line 1) and a concentrated (line 2) air parcel were simulated first. Then, four mixed air parcels were simulated. The mixed simulations were conducted for the dilution ratios of 1, 2, 4, and 8 (lines 3–6), respectively. The initial compositions of the air parcels are given in Table 2.

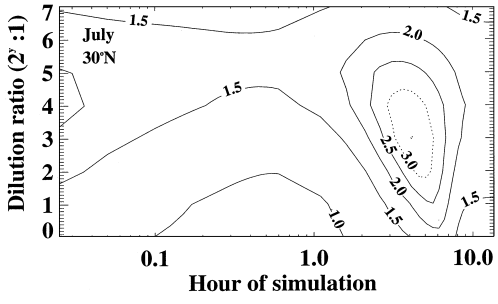

Fig. 2. The ratios of gross ozone production in the mixed simulations to those weighted sums in the isolated simulations for the fresh urban/baseline land case at 30°N in July. y denotes the labels in the y-axis.

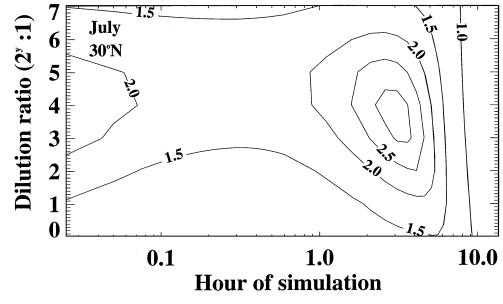

Fig. 3. The ratios of the net loss of NO_x in the mixed simulations to those weighted sums in the isolated simulations for the fresh urban/baseline land case at 30°N in July, y denotes the labels in the y-axis.

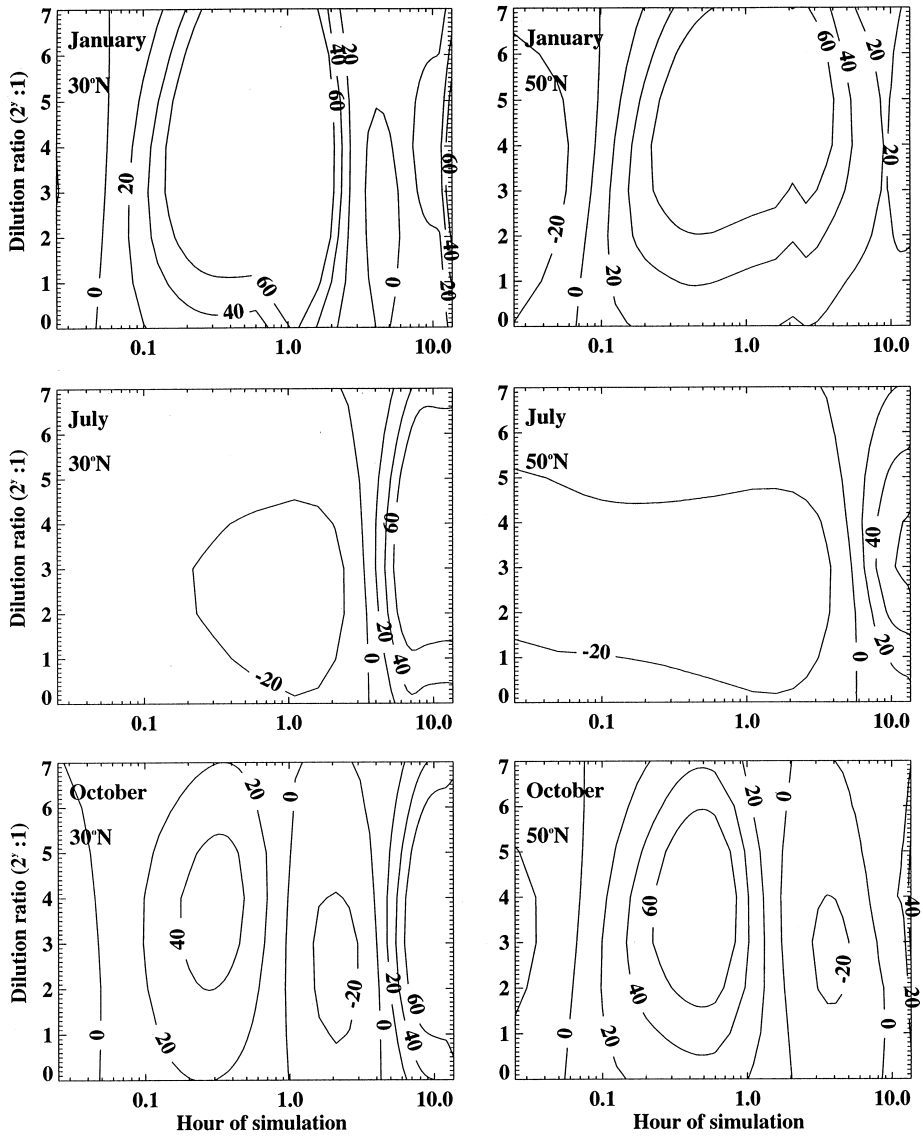

Fig. 4. The percentage difference between gross ozone production efficiencies in the mixed simulations and those weighted sums in the isolated simulations for the fresh urban/baseline land case at 30°N (left panel) and 50°N (right panel) in January (top panel), July (middle panel), and October (bottom panel). y denotes the labels in the y-axis.

efficiencies in the mixed simulations and those weighted sums in the isolated simulations for the fresh urban/baseline land case ranges from −20 to 60%, as shown in Fig. 4. The difference in ozone production efficiencies between the isolated and mixed simulations may be defined as errors resulting from the subgrid heterogeneity of an Eulerian model, which assumes ideal mixing within each grid cell. This finding suggests that the prediction of integrated ozone production may be overestimated by factors of up to 60% in a three-dimensional model at a variety of scales. Meanwhile, an Eulerian model that assumes complete mixing in a grid cell that contains segregated fresh urban and baseline land air parcels with a segregation time scale of less than a few hours, e.g., finely resolved urban airshed models, may underestimate integrated ozone production by 20% at mid- and high-latitudes in summer and in tropical area. Despite the difference in approach, Poppe et al. (1998) also found that in some cases ozone production integral decreases with dilution in the tropics.

The ratios of ozone production efficiencies in the mixed simulation to those in the isolated simulation varied with the composition of the air parcels. We show in Table 3 the ozone production efficiencies in the mixed case divided by the weighted sum of the ozone production efficiencies in the two isolated cases at the dilution ratio of 8 : 1 and an isolation time of 0.5 and 3 h for six cases. When the isolation time was 0.5 and 3 h, complete mixing underestimated ozone production efficiency by up to 30% in the fresh urban/baseline land case in subtropical and mid-latitude regions in summer. In other cases, complete mixing overestimated ozone production efficiency by up to threefold. These ratios do not show systematic difference between land and ocean airmasses, as shown in Table 3.

4. Conclusions

We compared the difference in ozone production efficiency when air masses of different origin were separated and when they were merged, using zero-dimensional simulations in various cases for several combinations of air mass origin, different latitudes, times of year, air mass dilution ratios and initial gas concentrations. We described that ozone production efficiency is a key parameter for evaluating the effect of anthropogenic NO_x on tropospheric ozone at a specific point in space, while the ozone production rate is a parameter appropriate for maximum ozone mixing ratio at a specific point in space and time. We estimated whether coarsely resolved models might under or overpredict ozone production due to their blending of air masses of different origin. We found that, under certain conditions, integrated ozone production may be overpredicted by as much as 60% in coarse-model grid cells exposed to different air masses. Under other conditions, such as in rather finely resolved urban airshed models, ozone production may actually be underpredicted by about 20% in mid-latitudes during summer. One implication of our results is that large-scale global models may have difficulty in correctly predicting ozone concentrations near, for instance, urban/free tropospheric boundaries, a conclusion supported by other studies.

Appendix A. Simple example of how ozone production efficiency may be either underestimated or overestimated

Consider a box x that contains two subboxes a and b with volumes of 10 and 1 generic units, respectively, If the mass of NO_x in subboxes a and b each is 1 generic unit, namely $M_{NO_x,a} = M_{NO_x,b} = 1$, then the mass of NO_x in the box x is 2, namely $M_{NO_x,x} = 2$. The NO_x concentration in each subbox may be denoted as c and $10c$ respectively, i.e., $[NO_x]_a = c, [NO_x]_b = 10c$. The

Table 3
Ratios of ozone production efficiencies in the mixed case to those in the isolated case at the dilution ratio of 8 : 1 and an isolation time of 0.5 and 3 h[a]

	Baseline urban/ Baseline land	Fresh urban/ Baseline land	Aged urban/ Baseline land	Baseline land/ Ocean	Forest land/ Ocean	Polluted land/Ocean
	0.5 h, 3.0 h	0.5 h, 3.0 h	0.5 h, 3.0 h	0.5 h, 3.0 h	0.5 h, 3.0 h	0.5 h, 3.0 h
At the Equator						
Jan.	1.36, 1.28	1.33, 0.89	1.26, 1.27	1.44, 1.80	1.42, 1.99	2.87, 2.55
Apr.	1.33, 1.31	1.29, 0.92	1.24, 1.28	1.46, 1.81	1.42, 2.04	2.86, 2.54
July	1.38, 1.25	1.36, 0.86	1.28, 1.27	1.48, 1.80	1.43, 1.93	2.93, 2.57
Oct.	1.34, 1.31	1.30, 0.92	1.26, 1.28	1.46, 1.80	1.42, 2.03	2.86, 2.53
At 30°N						
Jan.	2.85, 1.30	2.33, 1.06	3.28, 1.36	0.75, 1.84	0.59, 1.48	1.85, 2.85
Apr.	1.37, 1.18	1.36, 0.78	1.26, 1.28	1.49, 1.85	1.47, 1.84	3.02, 2.69
July	1.03, 1.36	0.74, 0.94	1.19, 1.30	1.63, 1.85	1.32, 2.15	2.46, 2.59
Oct.	1.37, 1.21	1.35, 0.82	1.26, 1.28	1.46, 1.83	1.45, 1.90	2.95, 2.64
At 60°N						
Jan.	2.00, 1.84	1.78, 1.59	2.31, 2.14	1.21, 1.44	1.06, 1.09	2.80, 3.62
Apr.	1.96, 1.12	1.93, 0.89	1.87, 1.27	1.78, 1.94	1.54, 1.52	4.02, 2.81
July	1.01, 1.11	0.71, 0.72	1.22, 1.26	1.85, 1.87	1.39, 1.71	2.50, 2.73
Oct.	1.98, 1.10	1.94, 0.85	1.86, 1.25	1.71, 1.89	1.56, 1.48	4.18, 2.74

[a]Cases and air parcels are defined in Table 2. The first and second column in each case is for isolation times of 0.5 and 3 h respectively.

NO_x concentration of box x, $[NO_x]_x$, is ($[NO_x]_a \times$ volume of subbox $a + [NO_x]_b \times$ volume of subbox b)/volume of box $x = (c \times 10 + 10c \times 1)/(10 + 1) = 20c/11$. The ozone production efficiencies of subboxes a and b are denoted as OPE_a and OPE_b, respectively. In the isolated case, the total ozone production of box x from all NO_x is $M_{NO_x,a} \times OPE_a + M_{NO_x,b} \times OPE_b = OPE_a + OPE_b$. Hence, the ozone production efficiency of the isolated case equals the total ozone production of the isolated case divided by the total loss of NO_x of the isolated case, or $(OPE_a + OPE_b)/2$. In the mixed case, the total ozone production efficiency of box x may be denoted as OPE_x. The difference of the total ozone production efficiency between the mixed case and the isolated case is

$$D = OPE_x - (OPE_a + OPE_b)/2. \quad (A.1)$$

To facilitate the discussion below, let us define

$$k = OPE_x \times [NO_x]_x. \quad (A.2)$$

Note that there is no implicit assumption about k, and that k may vary with time and locations, such as k in urban area may be different from that in background air.

When $OPE_a \times [NO_x]_a = OPE_b \times [NO_x]_b = k$, namely, the ozone production efficiency (OPE) is inversely proportional to the initial concentration of NO_x in each reservoir, then $OPE_x = k/[NO_x]_x = k/(20c/11)$, $OPE_a = k/[NO_x]_a = k/c$, and $OPE_b = k/[NO_x]_b = k/10c$. According to Eq. (A.1), $D = k/(20c/11) - (k/c + k/10c)/2 = 0$. Thus, the total ozone production efficiency of box x in the mixed case is the same as in the isolated case, and coarse grid models can precisely predict ozone production efficiency of box x without resolving subboxes a and b.

When $OPE_a \times [NO_x]_a > k$ and/or $OPE_b \times [NO_x]_b > k$, $D < k/(20c/11) - (k/c + k/10c)/2 = 0$ according to Eqs. (A.1) and (A.2). In this case, the total ozone production efficiency of box x in the mixed case is less than in the isolated case. Thus, coarse-grid models would underestimate ozone production efficiency of box x without resolving subboxes a and b.

When $OPE_a \times [NO_x]_a < k$ and/or $OPE_b \times [NO_x]_b < k$, $D > k/(20c/11) - (k/c + k/10c)/2 = 0$ according to Eqs. (A.1)–(A.2). In this case, the total ozone production efficiency of box x in the mixed case is larger than in the isolated case. Thus, coarse grid models would overpredict ozone production efficiency of box x without resolving subboxes a and b.

In sum, ozone production efficiency of a box with segregated airmasses may be either underestimated or overestimated by a model that assumes uniform mixing within the box.

References

Chameides, W.L., Fehsenfeld, F., Rodgers, M.O., Cardetino, C., Martinez, J., Parrish, D., Lonneman, W., Lawson, D.R., Rasmussen, R.A., Zimmerman, P., Greenberg, J., Middleton, P., Wang, T., 1992. Ozone precursor relationship in the ambient atmosphere. Journal of Geophysical Research 97, 6037–6055.

Chatfield, R.B., Delany, A.C., 1990. Convection links biomass burning to increased tropical ozone: however, models will tend to overpredict O_3. Journal of Geophysical Research 95, 18473–18488.

Hilst, G.R., 1998. Segregation and chemical reaction rates in air quality models. Atmospheric Environment 32, 3891–3895.

Horowitz, L.W., Jinyou Liang, Gardner, G.M., Jacob, D.J., 1998. Export of reactive nitrogen from North America during summertime: sensitivity of hydrocarbon chemistry. Journal of Geophysical Research 103, 13451–13476.

Jacob, D.J., Logan, J.A., Yevich, R.M., Gardner, G.M., Spivakovsky, C.M., Wofsy, S.C., Munger, J.W., Sillman, S., Prather, M.J., Rodgers, M.O., Westberg, H., Zimmermann, P.R., 1993. Simulation of summertime ozone over North America. Journal of Geophysical Research 98, 14797–14816.

Jang, J.C.C., Jeffries, H.E., Tonnesen, S., 1995. Sensitivity of ozone to model grid resolution II. detailed process analysis for ozone chemistry. Atmospheric Environment 29, 3101–3114.

Liang, J.Y., Jacob, D.J., 1997. Effect of aqueous-phase cloud chemistry on tropospheric ozone. Journal of Geophysical Research 102, 5993–6001.

Liang, J.Y., Jacobson, M.Z., 1999. A study of sulfur dioxide oxidation pathways over a range of liquid water contents, pH values, and temperatures. Journal of Geophysical Research 104, 13749–13769.

Liang, J.Y., Horowitz, L.W., Jacob, D.J., Wang, Y., Fiore, A.M., Logan, J.A., Gardner, G.M., Munger, J.W., 1998. Seasonal budgets of reactive nitrogen species and ozone over the United States, and export fluxes to the global atmosphere. Journal of Geophysical Research 103, 13435–13450.

Lin, X., Trainer, M., Liu, S.C., 1988. On the nonlinearity of the tropospheric ozone production. Journal of Geophysical Research 93, 15879–15888.

Liu, S.C., Trainer, M., Fehsenfeld, F.C., Parrish, D.D., Williams, E.J., Fahey, D.W., Hubler, G., Murphy, P.C., 1987. Ozone production in the rural troposphere and the implications for regional and global ozone distributions. Journal of Geophysical Research 92, 4191–4207.

Makar, P.A., Polavarapu, S.M., 1997. Analytic solutions for gas-phase chemical mechanism compression. Atmospheric Environment 31, 1025–1039.

Poppe, D., Koppmann, R., Rudolph, J., 1998. Ozone formation in biomass burning plumes: influence of atmospheric dilution. Geophysical Research Letters 25, 3823–3826.

Sillman, S., Logan, J.A., Wofsy, S.C., 1990. A regional scale model for ozone in the United States with subgrid representation of urban and power plant plumes. Journal of Geophysical Research 95, 5731–5748.